Journal of Solid State Chemistry **152,** 568–572 (2000)
doi:10.1006/jssc.2000.8740, available online at http://www.idealibrary.com on IDEAL®

RAPID COMMUNICATION

X-Ray Diffraction Pattern Simulation for Thermally Treated [Zn–Al–Cl] Layered Double Hydroxide

A. Ennadi,*,[1] A. Legrouri,† A. De Roy,‡ and J. P. Besse‡

*Laboratoire de Chimie-Physique, Faculté des Sciences Semlalia, Université Cadi Ayyad, B.P. 2390, Marrakech 40001, Morocco;
†School of Science & Engineering, Al Akhawayn University, P.O. Box 1871, Ifrane 53000, Morocco; and ‡Laboratoire des Matériaux Inorganiques, UPRES-A 6002, Université Blaise Pascal, 63177, Aubière-Cedex, France

Received February 8, 2000; in revised form March 23, 2000; accepted April 7, 2000

Thermal analyses and X-ray diffraction (XRD) were combined with refinement and simulation of the XRD patterns in order to elucidate the evolution of the atom distribution in the interlayer domain of the [Zn–Al–Cl] layered double hydroxide during heating. Rietveld refinement indicates that the structure is composed of $[Zn_{1-x}Al_x(OH)_2]^{0.33+}$ layers separated by water molecules and chloride ions. Zn and Al are randomly distributed among the octahedral positions. The OH layer sequence is –BC–CA–AB–BC–. Oxygen of water molecules and chloride ions, also randomly distributed, prefer positions at about 0.76 Å of the threefold axis. The simulation of the XRD patterns shows that these positions were imposed by geometric constraints of water molecules connecting two OH groups of adjacent brucite-like layers.

Key Words: **layered double hydroxides; structure; interlayer; X-ray diffraction; refinement; simulation.**

I. INTRODUCTION

Layered double hydroxides (LDHs) of the general formula (1)

$$[M^{II}_{1-x}M^{III}_x(OH)_2]^{x+}[X^{y-}_{x/y}\cdot nH_2O]^{x-}$$

symbolized by $[M^{II}–M^{III}–X]$

are characterized by $M(OH)_2$ layers formed by an association of edge-sharing coplanar octahedra. The presence of a trivalent metal implies a positive charge for the layers, which is counterbalanced by the presence of hydrated anions between these layers. LDHs exist as minerals but are also synthesized by various methods based mainly on the controlled coprecipitation of metallic salts (2).

The only structural studies on single crystals for these compounds were performed on minerals (3–6). The impossibility of obtaining suitable synthetic single crystals renders their structural analysis by XRD very delicate. However, the Rietveld method (7,8) makes it possible to solve some crystalline structures of LDHs from powder XRD data (9–12).

In these compounds, if the structure of the hydroxylated $M(OH)_2$ brucite-like layers is well known, the organization of matter in the interlayer domain is, in contrast, less well defined. The work described in this paper was undertaken in order to locate the interlayer atoms in a [Zn–Al–Cl] LDH phase, by combining thermogravimetric analysis (TGA) and differential thermal analysis (DTA) with XRD to the refinement and simulation of the powder XRD patterns. The selection of the [Zn–Al–Cl] system among other LDHs was related to the better crystalline organization that could be obtained. The studied compound has a trivalent metal ratio $x = 1/3$.

II. MATERIALS AND METHODS

The starting material, [Zn–Al–Cl], was prepared following the standard coprecipitation method described by Miyata (2). Aqueous solution containing $ZnCl_2$ and $AlCl_3.6H_2O$ ($Zn^{II}/Al^{III} = 2$) was slowly introduced under stirring in a reactor containing freshly deionized water. The pH was maintained constant at 8.5 by the simultaneous addition of NaOH. The resulting slurry was then left under stirring for 24 h. The precipitate was filtered, and washed several times with water. It was then dried in air at ambient temperature. For the prepared compound, chemical analysis and TGA are in agreement with the following formula: $Zn_{2/3}Al_{1/3}(OH)_2Cl_{1/3}\cdot\frac{2}{3}H_2O$.

[1] To whom correspondence should be addressed. Permanent address: Département de Physique, Faculté des Sciences et Techniques, Université Sidi Mohamed Ben Abdellah, B.P. 2202, Fès 30000, Morocco.

0022-4596/00 $35.00

Simultaneous DTA and TGA experiments were performed on a Setaram TGA 92 instrument. Curves were recorded from ambient temperature up to 1030°C at a rate of 5°C/min under a 17% relative humidity air flow and using 20 mg of the sample, which was initially in equilibrium with this air flow.

The XRD equipment used was a Siemens D 501 diffractometer. Samples were rotated while being exposed to Cu $K\alpha$ radiation. All samples were passed though a 100-μm sieve before the filling of the sample holder by using McMurdie's method (13) in order to avoid preferential orientation. During data collection, the sample holder was rotating at the speed of 30 revolutions per minute.

Powder XRD patterns were recorded at room temperature from original precipitate and later from samples heated at 100, 130, 150, 180 and 240°C for 24 h, upon cooling. Measurement conditions were 2θ range, 2–76°; step size, 0.08° 2θ; step counting time, 4 s. For powder XRD patterns from original precipitate, used for structural refinement, the analysis conditions were 2θ range, 5–105°; step size, 0.04° 2θ; step counting time, 20 s.

Software based on the formalism of Debye (14) was applied for the XRD pattern simulation. The position of every atom in the unit cell is drawn directly from structure refinement data obtained by the method of Rietveld. A volume of 50 unit cells along a and b and 5 unit cells along c was sufficient to get a good definition of the XRD lines (9).

III. RESULTS AND DISCUSSION

1. Structural Evolution

The thermal decomposition of the synthetic [Zn–Al–Cl] compounds was investigated by TGA–DTA and XRD. TGA–DTA diagrams (Fig. 1) are quite similar to those obtained and reported in previous works (15,16); i.e., two steps of weight loss were observed, the first attributed to the loss of interlayer water, which is complete at about 200°C, and the second to dehydroxylation (collapse of the lamellar structure at 240°C) leading to the formation of zinc oxide (ZnO) and a spinel phase ($ZnAl_2O_4$) at higher temperatures.

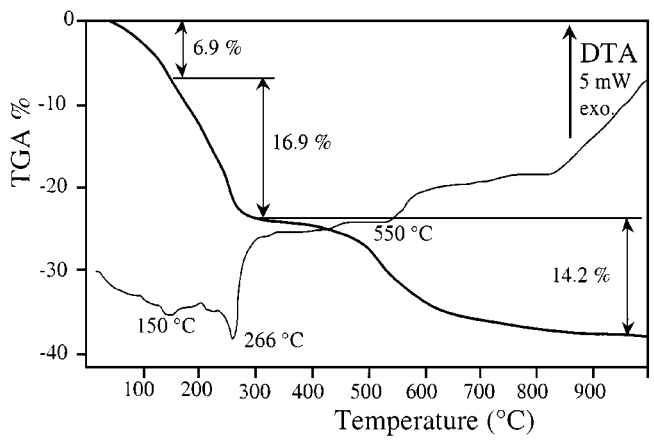

FIG. 1. DTA and TGA curves for [Zn–Al–Cl].

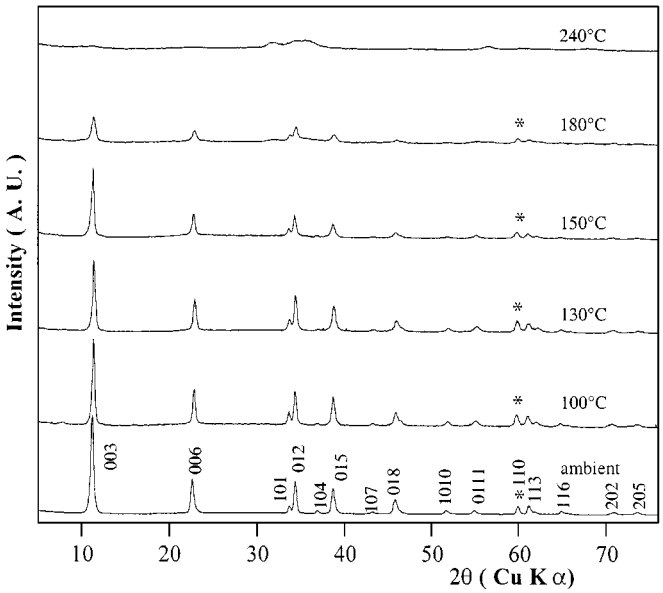

FIG. 2. XRD patterns for [Zn–Al–Cl] at different temperatures.

XRD patterns of heated phases are shown in Fig. 2. The study was limited to samples heated up to 180°C, since complete thermal decomposition occured at 240°C. The XRD patterns corresponding to the rhombohedral symmetry (space group, R-3m), were indexed in an hexagonal lattice. The a and c lattice parameters were estimated using (110) and (003) reflections, respectively. In the studied temperature domain, the evolution of chemical composition is described by n, the number of interlamellar water molecules. It is obtained from the TGA data. Another suitable parameter is the basal spacing of the layers $d = c/3$. These parameters and the cell parameters are listed in Table 1 for each stage of thermal treatment. The interlayer distance d decreases when the temperature is raised to 130°C. After this temperature, an inverse evolution was noted at 150°C

TABLE 1
Cell Parameters and Composition of the Phases at Different Temperatures

T (°C)	a (nm)	c (nm)	n	d (nm)
Ambient	0.3091	2.354	0.66	0.783
100	0.3089	2.314	0.57	0.771
130	0.3087	2.302	0.44	0.767
150	0.3086	2.331	0.31	0.777
180	0.3079	2.314	0.13	0.771

followed by another decrease at 180°C. A similar evolution was observed in previous work (17) and a phase transition was suggested. The *a* parameter decreases weakly but steadily.

2. Structure Refinement and Discussion

The Rietveld–Le Bail profile refinement method (18,19) was used to obtain a structural model for the studied compound before thermal treatment. The structure of the studied phase was refined as isotypic of the rhombohedral pyroaurite (4). The structure is built up of brucite-like $[(Zn^{II}_{0.66}Al^{III}_{0.33})(OH)_2]^{0.33+}$ layers with a –BC–CA–AB–BC– sequence for the successive OH layers, with a disordered distribution of metallic cations. These main layers are separated by disordered interlayer domains $[1/3Cl + 2/3H_2O]^{0.33-}$, where Cl^- anions and H_2O molecules are also statistically distributed. The site occupancies have been fixed according to the nominal composition.

The structure refinement was initiated by building octahedral coordination for metallic cations. The metals are distributed on the 3(*a*) (0,0,0) position of the *R*-3*m* space group. The hydroxyl groups are located on particular position 6(*c*) (0,0,0.37) ($\bar{9}$,$\bar{2}0$,21). The interlayer domain species were first placed at 3(*b*) (0,0,1/2). This position led to a high thermal vibration perpendicular to the [001] direction; the anisotropic temperature factors were $B_{11} = 34.6$ Å^2 and $B_{33} = 3.3$ Å^2. The final reliability factors were $R_I = 6.2\%$ and $R_{WP} = 15.32\%$. In order to reduce these temperature factors and get a better refinement, attempts were made by distributing the interlayer domain species over higher multiplicity sites corresponding to six positions around the C_3 axis of the space group. The positions 18(*g*) (*x*,0,1/2), with refined $x = 0.248$, and 18(*h*) ($x, -x, z$), with refined $x = 0.129$, $z = 1/2$, were checked. For both hypothesis the parameters of (Zn,Al) and OH did not significantly change in this refinement, but for (Cl, H_2O)B_{11} became 17.3 Å^2 and 18.2 Å^2 for 18(*g*) and 18(*h*) positions, respectively. The reliability factors were also improved and very similar for the two cases. The refinement results for the three structural hypothesis are reported in Table 2. The experimental, calculated with 18(*g*) position, and difference patterns are shown in Fig. 3.

Scattering factors for Al^{3+}, Zn^{2+}, and Cl^- were taken from *International Tables for X-Ray Crystallography* (22). The H_2O molecules and OH^- ions were considered as O^{2-} ions which scattering factors taken from Suzuki (23).

3. Simulation of XRD Patterns

The position of each atom in the unit cell was taken from the data resulting from structural refinement. The simulations of the XRD patterns considering the 18(*g*) and 3(*b*) positions for atoms of interlayer domain compared with experimental XRD pattern are shown in Fig. 4. It was noticed that the simulation considering the position 18(*g*) gave the best results; nevertheless, the intensity of the (110)

TABLE 2
Structural Parameters for [Zn–Al–Cl] at Ambient Temperature for Three Positions

	Interlayer atoms at 3(*b*)	Interlayer atoms at 18(*g*)	Interlayer atoms at 18(*h*)
(Zn,Al) at position	3(*a*): (0,0,0)	3(*a*): (0,0,0)	3(*a*): (0,0,0)
B_{11} (Å^2)	2.9(2)	2.3(2)	2.5(1)
B_{33} (Å^2)	4.5(3)	5.5(2)	4.8(3)
OH at position	6(*c*): (0,0,*z*)	6(*c*): (0,0,*z*)	6(*c*): (0,0,*z*)
	$z = 0.3772(3)$	$z = 0.3775(1)$	$z = 0.3775(2)$
B_{11} (Å^2)	2.6(5)	2.6(2)	3.1(4)
B_{33} (Å^2)	5.4(5)	4.3(3)	5.1(4)
(Cl,H_2O) at position	3(*b*): (0,0,1/2)	18(*g*): (*x*,0,1/2)	18(*h*): ($x, -x, z$)
		$x = 0.248(5)$	$x = 0.129(2)$,
			$z = 1/2$
B_{11} (Å^2)	34.6(2)	17.3(10)	18.2(11)
B_{33} (Å^2)	3.3(4)	2.5(4)	2.7(5)
Cell parameters			
a (Å)	3.085(3)	3.083(1)	3.084(2)
c (Å)	23.48(5)	23.47(5)	23.47(6)
Reliability factors			
R_I (%)	6.20	4.95	5.15
R_{WP} (%)	15.32	13.25	13.52

Note. $B_{11} = B_{22} = 2B_{12}$.

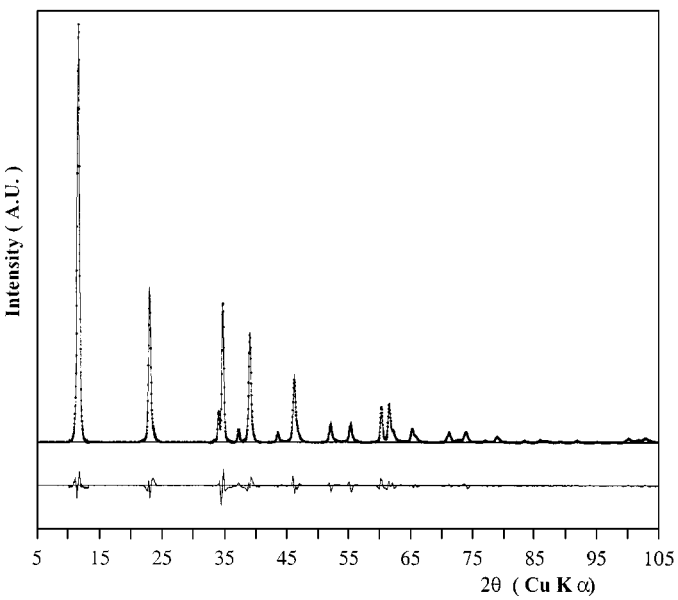

FIG. 3. Experimental, calculated, and difference powder XRD patterns at ambient temperature.

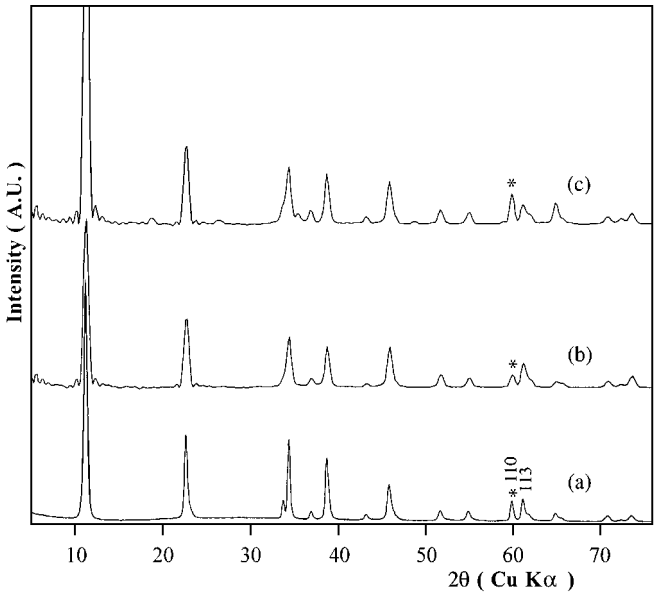

FIG. 4. Simulated XRD patterns with interlayer atoms in position 3(*b*) (c) 18(*g*) (b) compared to those of experimental (a).

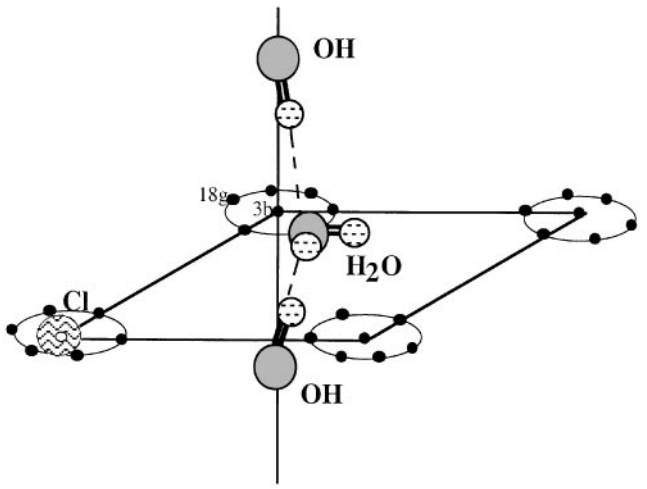

FIG. 5. Hypothesis for atom distribution in the interlayer domain.

line of the simulated pattern stays relatively low with respect to the experimental pattern. In addition, it was noticed that the (110) line intensity is very sensitive to the 3(*b*) position. This study allows to propose the main following hypothesis:

Encumbrance of interlayer domains can be related to water molecules. In fact, the structure description shows that the 3(*b*) positions are located exactly between two hydroxyl groups belonging to two neighboring brucitic layers. In order to ensure hydrogen bonding with these hydroxyl groups, water molecules, which should normally occupy the most symmetrical position 3(*b*), occupy the adjoining space of this position while respecting distances and angles for hydrogen bonding. The chloride anion, which does not present any particular geometric constraints, has a tendency to occupy the 3(*b*) position, but it is unsettled due the encumbrance of water molecules. This leads probably to very strong oscillations of the anion around the equilibrium position of 3(*b*). This hypothesis is illustrated by Fig. 5.

The simulation of XRD patterns for heated samples was limited to temperatures between the ambient and 150°C. Due to strong thermal degradation, the sample heated at 180°C appeared not suitable for such comparisons. The construction of models for the solids to be simulated was undertaken as follows:

— The structure of hydroxylated layers was described from atomic positions previously obtained by Rietvelt analysis.

— The interlayer domains were modelled by taking into account the atomic positions for Cl^- and H_2O species and their occupancies in agreement with TGA.

The simulated diffraction patterns show that the intensity of the (110) line increases with the ratio of the 3(*b*) site occupancy, while the 18(*g*) and 18(*h*) positions do not influence such intensity. Analysis of XRD patterns of heated products (Fig. 2) indicates that the intensity of the (110) line increases with temperature. This is in agreement with our hypothesis of progressive location of chlorides on the 3(*b*) position related to the loss of water molecules.

Let us consider the $Zn_{2/3}Al_{1/3}(OH)_2Cl_{1/3}.0.66H_2O$ starting formula with all interlayer species in 18(*g*) (0.248,0,1/2) and the corresponding hypothetical fully dehydrated compound $Zn_{2/3}Al_{1/3}(OH)_2Cl_{1/3}$ with interlayer chloride in 3(*b*) (0,0,1/2). An elementary hypothesis considers a linear combination of these two extreme interlayer occupancies in order to simulate the heated compounds characterized by their actual hydration ratio $0.66 > n > 0.31$. In fact, the simulated patterns obtained in this way (Fig. 6) display a clear evolution of the relative intensities of (110) and (113) lines. A very similar evolution is observed on the experimental patterns of the thermally treated samples (Fig. 2).

IV. CONCLUSION

Simulation of XRD patterns applied to [Zn–Al–Cl] phases, having undergone thermal treatment, has shown an evolution of the atom distribution in the interlayer domain.

In the course of dehydration, matter is progressively brought together around the threefold axis and stands between the hydroxyl groups of neighboring layers. This evolution can be attributed to the progressive disappearance of geometric constraints imposed by the presence of water molecules, which establish hydrogen bonding with the hydroxylated layers.

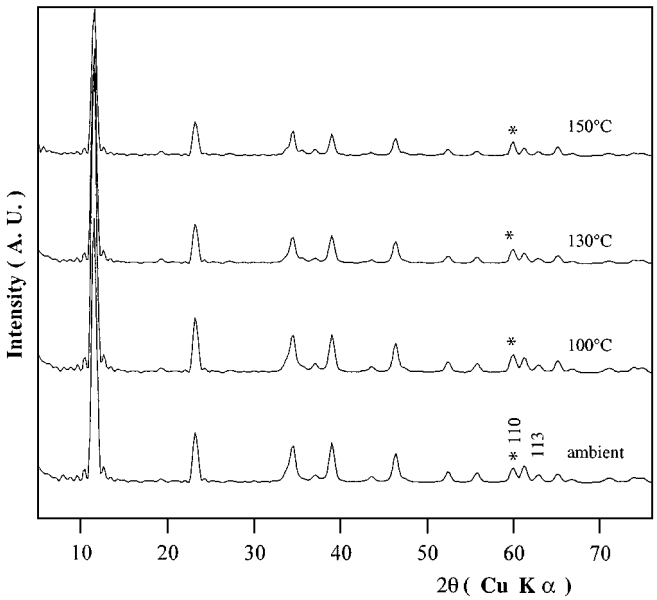

FIG. 6. Simulated XRD patterns at different temperatures.

For other systems such as [Zn–Cr–Cl], the evolution of the basal spacing on heated samples display similar features which could also be related to structural modifications in the interlayer domain (16). Therefore, we are looking for other LDH systems with this behavior. The choice of interlayer anions heavier than chloride would increase the sensitivity of the method for further studies.

REFERENCES

1. A. de Roy, C. Forano, K. El Malki, and J. P. Besse, *in* "Synthesis of Microporous Materials" (M. L. Occelli and H. E. Robson, Eds.), Vol. 2, Chap. 7, p. 108, Van Nostrand Reinhold, New York, 1992.
2. S. Miyata, *Clays Clay Miner.* **23,** 369 (1975).
3. L. Ingram and H. F. W. Taylor, *Mineral. Mag.* **36,** 465 (1967).
4. R. Allmann, *Acta Crystallogr. B* **24,** 972 (1968).
5. R. Allmann, *N. Jb. Miner. Mh.* 552 (1969).
6. J. Rius and R. Allmann, *Z. Kristallogr.* **168,** 133 (1984).
7. H. M. Rietveld, *Acta Crystallogr.* **20,** 508 (1966).
8. H. M. Rietveld, *J. Acta Crystallogr.* **2,** 65 (1968).
9. A. Ennadi, Thesis, Blaise Pascal University, Clermont-Ferrand, France, 1993.
10. A. Ennadi, M. Khaldi, A. de Roy, and J. P. Besse, *Mol. Cryst. Liq. Cryst.* **244,** 373 (1994).
11. J. P. Thiel, C. K. Chiang, and R. Poeppelmeier, *Chem. Mater.* **5,** 297 (1993).
12. M. Bellotto, B. Rebours, O. Clause, J. Lynch, D. Bazin, and E. Elkaim, *J. Phys. Chem.* **100,** 8527 (1996).
13. M. F. Mc Murdie, M. C. Morris, E. H. Evans, B. Paretzkin, W. Wong-Ng, and C. R. Hubbard, *Powder Diffraction* **1,** 40 (1986).
14. D. Espinat, E. Godart, and F. Thevenot, *Analysis* **15,** 337 (1987).
15. K. El Malki, A. De Roy, and J. P. Besse, *Eur. J. Solid State Inorg. Chem.* **26,** 339 (1989).
16. A. De Roy, A. M. Vernay, J. P. Besse, and G. Thomas, *Analysis* **16,** 409 (1988).
17. A. de Roy, J. P. Besse, and P. Bondot, *Mater. Res. Bull.* **20,** 1091 (1985).
18. A. Le Bail, *10th Coll. Rayons X Siemens*, Grenoble, 1985.
19. C. Lartigue, A. Le Bail, and A. Percheron-Guegan, *J. Less-Common Met.* **129,** 65 (1987).
20. A. de Roy, "Thesis, Doctorat d'Etat, Blaise Pascal University, Clermont-Ferrand, France, 1990.
21. A. de Roy, *Mol. Cryst. Liq. Cryst.* **311,** 173 (1998).
22. "International Tables for Crystallography," Vol. IV, Kluwer, Dordrecht, 1974.
23. T. Suzuki, *Acta Crystallogr.* **13,** 279 (1960).